Dynamically active compartments coupled by a stochastically-gated gap junction

Paul C. Bressloff[1], Sean D. Lawley[1]

[1] *Department of Mathematics, University of Utah, Salt Lake City, UT 84112 USA*

Abstract

We analyze a one-dimensional PDE-ODE system representing the diffusion of signaling molecules between two cells coupled by a stochastically-gated gap junction. We assume that signaling molecules diffuse within the cytoplasm of each cell and then either bind to some active region of the cell's membrane (treated as a well-mixed compartment) or pass through the gap junction to the interior of the other cell. We treat the gap junction as a randomly fluctuating gate that switches between an open and a closed state according to a two-state Markov process. This means that the resulting PDE-ODE is stochastic due to the presence of a randomly switching boundary in the interior of the domain. It is assumed that each membrane compartment acts as a conditional oscillator, that is, it sits below a supercritical Hopf bifurcation. In the ungated case (gap junction always open), the system supports diffusion-induced oscillations, in which the concentration of signaling molecules within the two compartments are either in-phase or anti-phase. The presence of a reflection symmetry (for identical cells) means that the stochastic gate only affects the existence of anti-phase oscillations. In particular, there exist parameter choices where the gated system supports oscillations but the ungated system does not, and vice-versa. The existence of oscillations is investigated by solving a spectral problem obtained by averaging over realizations of the stochastic gate.

Keywords: gap junctions, diffusion, piecewise deterministic PDEs, channel permeability

1. Introduction

An important problem in cell biology is understanding intracellular and intercellular communication [2]. This typically involves a signaling molecule that diffuses in the cytoplasm (aqueous interior) of an individual cell or in the intercellular space between cells, and subsequently binds to a receptor on the plasma

Email addresses: bresslof@math.utah.edu (Paul C. Bressloff[1]), lawley@math.utah.edu (Sean D. Lawley[1])

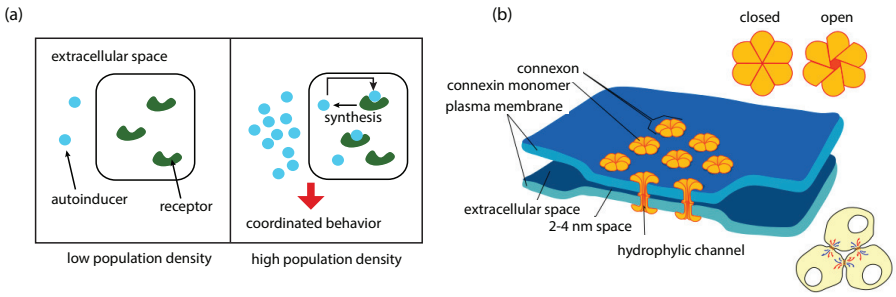

Figure 1: Two forms of intercellular communication. (a) A schematic illustration of quorum sensing at the single-cell level. (b) Schematic diagram of gap junction coupling between two cells. [Public domain figure downloaded from Wikimedia Commons.]

membrane of a cell, triggering a signaling cascade. One example of an intercellular signaling mechanism is bacterial quorum sensing [32, 38], see Fig. 1(a). Quorum sensing involves the production and extracellular secretion of certain signaling molecules known as autoinducers. Each cell has receptors that can specifically detect the signaling molecule and subsequently activate the transcription of certain genes, including those for inducer synthesis. However, since there is a low likelihood of an individual bacterium detecting its own secreted inducer, the cell must encounter signaling molecules secreted by other cells in its environment in order for gene transcription to be activated. This in turn requires the cell density to be sufficiently high. That is, as the cell population grows, the concentration of the inducer passes a threshold, causing more inducer to be synthesized. This generates a positive feedback loop that induces the up-regulation of other specific genes. Hence, all of the cells initiate transcription at approximately the same time, resulting in some form of coordinated behavior such as synchronized oscillations. It should be noted, however, that most models of bacterial quorum sensing are based on deterministic ordinary differential equations (ODEs), in which both the individual cells and the extracellular medium are treated as well-mixed compartments (fast diffusion limit) [26, 9]. (For a discussion of spatial models that take into account bulk diffusion of the autoinducer in the extracellular domain see Refs. [33, 34])

Another form of intercellular communication is via gap junctions [17, 36, 20], see Fig. 1(b). These are arrays of transmembrane channels that connect the cytoplasm of two neighboring cells and thus provide a direct diffusion pathway between the cells. Cells sharing a gap junction channel each provide a hemichannel (also known as a connexon) that connect head-to-head. The physiological properties of a gap junction, including its permeability and gating characteristics, are determined by the particular connexins forming the channel. Gap junctions have been found in almost all animal organs and tissues, and allow for direct electrical and chemical communication between cells [12, 25]. Direct chemical communication between cells occurs through the transmission of small second messengers, such as inositol triphosphate (IP3) and calcium (Ca^{2+}) that

can then trigger self-sustained intercellular oscillations and waves through processes such as calcium-induced-calcium-release.

Both of the examples above involve the coupling between bulk diffusion of a signaling molecule and biochemical processes occurring within a more restricted domain such as the membrane of a cell or some intracellular organelle. Often the latter can be treated as a well-mixed (non-spatial) compartment. This type of coupling has recently been investigated in a series of papers by Gou et al [21, 22, 23, 24], see also Sancho et al. [19]. In particular Gou et al. have analyzed the synchronization of two or more biological oscillators coupled by bulk diffusion. Each oscillator is treated as a well-mixed compartment that can exchange signaling molecules with the bulk domain. The concentration of signaling molecules within each compartment is modeled by a system of nonlinear ODEs while the concentration in the bulk medium is modeled by a partial differential equation (PDE) for diffusion and degradation. Gou et al. assume that each isolated compartment is a conditional oscillator. That is, in isolation a compartment's dynamics is at a stable fixed point, but can exhibit sustained oscillations in a different parameter regime. Using spectral theory and a winding number analysis, the authors showed that in the case of a pair of active compartments, diffusive coupling can induce in-phase or anti-phase oscillations. This analysis has also been extended to the case of diffusively coupled delay-differential equations (DDEs) [40].

In this paper, we combine the analysis of PDE-ODE systems with our own recent work on diffusion in cells with stochastically-gated gap junctions [7, 8]. We assume that signaling molecules diffuse within the cytoplasm of each cell and then either bind to some active region of the cell's membrane (treated as a well-mixed compartment) or pass through the gap junction to the interior of the other cell. Just as with the opening and closing of ion channels, gap junctions can be gated by both voltage and chemical agents, both of which can fluctuate. Therefore, following [7, 8], we treat the gap junction as a randomly fluctuating gate that switches between an open and a closed state according to a two-state Markov process. This means that the resulting PDE-ODE is stochastic due to the presence of a randomly switching boundary in the interior of the domain. For simplicity, we consider a one-dimensional (1D) domain of length $2L$, with L the length of each cell. The switching gate is placed at the center of the domain ($x = L$), whilst the active compartments are placed at the ends ($x = 0, 2L$). Deterministic boundary conditions at the two ends represent the exchange of signaling molecules between the bulk and the active compartments, whereas the boundary condition at the midline randomly switches between open and closed.

One of the particular features of the stochastically-gated model is that it has a deterministic steady-state solution that is symmetric about the midline $x = L$, which is identical to the steady-state solution considered by Gou et al [21, 22]. Linearizing about this steady-state solution generates a stochastic linear PDE-ODE for pertubations about the steady state. We analyze the latter by extending our recent work on diffusion in bounded domains with randomly switching boundaries [27, 3, 7, 8]. That is, we spatially discretize the stochastic diffusion equation using finite differences and construct the Chapman-Kolmogorov (CK)

equation for the resulting finite-dimensional piecewise deterministic ODE, also known as a stochastic hybrid system [2]. This allows us to derive a deterministic equation for the first-order moments of the stochastic concentrations with respect to realizations of the stochastic gate (after re-taking the continuum limit), which take the form of a deterministic linear PDE-ODE. We then solve the resulting spectral problem following along analogous lines to Gou et al. [21, 22]. This yields a restricted stability criterion, namely, that the resulting spectrum has to lie in the left-half complex plane. We emphasize that it is restricted because we are using the first moments of a linearization to predict the behavior of a stochastic nonlinear system. Nevertheless, predictions of this restricted theory are consistent with numerical simulations of the full nonlinear stochastic system.

These numerically-confirmed predictions are the following: First, as in the ungated case considered by Gou et al [21, 22], oscillations occur over a finite range of diffusivities that excludes the origin, indicative of diffusion-induced oscillations. Second, the existence of in-phase oscillations is not affected by the presence of a stochastic gate because the flux through the midline $x = L$ is zero. However, the existence of anti-phase oscillations is affected. In particular, we find that if switching is sufficiently fast or the gate is mainly open, then the anti-phase existence region of the gated system approaches the corresponding region of the ungated system. On the other hand, if the gate is mainly closed, then the anti-phase region of the gated system approaches the in-phase region. For intermediate switching rates, the anti-phase region of the gated system seems to interpolate between the anti-phase and in-phase regions of the ungated system. In that case, there exist parameter choices where the gated system supports oscillations, but the ungated system does not, and there exists parameter choices where the converse holds.

2. A pair of active compartments coupled by a stochastically-gated gap junction

Consider a simple 1D model that describes the diffusion and degradation of a signaling molecule that can pass between two cells of length L via a stochastically-gated gap junction, see Fig. 2. Let $u(x,t)$ denote the bulk concentration of the signaling molecules at time t with $x \in [0, 2L]$. Two identical active compartments are introduced at the distal ends of the cells, $x = 0, 2L$. We assume that the interior boundary between the two cells at $x = L$ randomly switches between an open and a closed state. Let $n(t)$ denote the discrete state of the gate at time t with $n(t) = 0$ if the gate is open and $n(t) = 1$ if it is closed. Assume that transitions between the two states $n = 0, 1$ are described by the two-state Markov process,

$$0 \underset{\alpha}{\overset{\beta}{\rightleftharpoons}} 1,$$

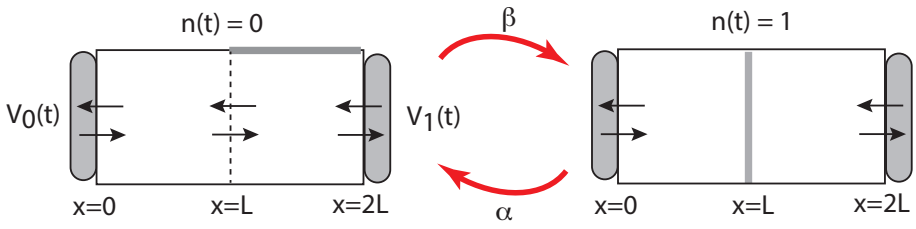

Figure 2: Pair of cells of length L that are coupled by a stochastically-gated gap junction at $x = L$, which stochastically switches between an open and a closed state according to a two-state Markov process with transition rates α, β.

The random opening and closing of the gate means that particles diffuse in a random environment according to the piecewise deterministic equation

$$\frac{\partial u}{\partial t} = D\frac{\partial^2 u}{\partial x^2} - \gamma u(x,t) \tag{2.1a}$$

where D is the diffusion coefficient and γ the degradation rate. The concentration $u(x,t)$ satisfies the exterior boundary conditions

$$-Du_x(0,t) = \kappa(V_0(t) - u(0,t)), \quad Du_x(2L,t) = \kappa(V_1(t) - u(2L,t)), \tag{2.1b}$$

where $V_r(t)$, $r = 0, 1$, are the concentrations of the particle in the two end compartments. For simplicity, we assume that the flux of particles out of each compartment is proportional to the difference between the concentration inside each compartment and the local bulk concentration. Finally, there is an $n(t)$-dependent boundary condition on the interior boundary at $x = L$:

$$u(L^-,t) = u(L^+,t), \quad \partial_x u(L^-,t) = \partial_x u(L^+,t) \quad \text{for } n(t) = 0, \tag{2.1c}$$

and

$$\partial_x u(L^-,t) = 0 = \partial_x u(L^+,t) \quad \text{for } n(t) = 1, \tag{2.1d}$$

where we use $f(y\pm)$ to denote the limit from the left or right, $\lim_{x\to y\pm} f(x)$. That is, when the gate is open there is continuity of the concentration and the flux across $x = L$, whereas when the gate is closed the right-hand boundary of the first cell and the left-hand boundary of the second cell are reflecting. For simplicity, we assume that the diffusion coefficient is the same in both compartments so that the piecewise differentiable nature of the solution is solely due to the switching gate.

The dynamics governing the time evolution of the concentration $V_r(t)$ couples the concentration with another variable $W_r(t)$ according to the following system of nonlinear ODEs:

$$\frac{dV_r}{dt} = F(V_r, W_r) + \overline{\kappa}[u(2Lr,t) - V_r(t)], \quad \frac{dW_r}{dt} = G(V_r, W_r). \tag{2.2}$$

Following Gou et al [21, 22], we assume that the intrinsic dynamics and the diffusive coupling term are identical for the two compartments. Furthermore,

both compartments are taken to act as conditional limit cycle oscillators. That is, there exists a parameter regime for each isolated compartment ($\beta = 0$) for which the second-order nonlinear ODE $\dot{V} = F(V, W)$, $\dot{W} = G(V, W)$ supports limit cycle oscillations. However, we assume that each isolated compartment is outside this parameter regime, and has a unique stable fixed point. We are interested in determining conditions under which the coupled system supports stochastic oscillations.

2.1. Symmetric steady-state solution

One of the particular features of the stochastically-gated model is that it has a deterministic steady-state solution that is symmetric about the midline $x = L$, which is identical to the steady-state solution considered by Gou et al [21, 22] (we are considering only symmetric steady-states, though asymmetric steady states can exist in certain situations, see equations (3.27)-(3.29) of [22]). That is, we impose the condition $\partial_x u(L) = 0$ independently of n, so that equation (2.1a) reduces to the deterministic, time-independent equation

$$D\frac{d^2U^{\rm ss}}{dx^2} - \gamma U^{\rm ss} = 0, \tag{2.3}$$

for $x \in [0, L]$ with boundary conditions

$$-D\left.\frac{dU^{\rm ss}}{dx}\right|_{x=0} = \kappa(V^{\rm ss} - U^{\rm ss}(0)), \quad \left.\frac{dU^{\rm ss}}{dx}\right|_{x=L} = 0, \tag{2.4}$$

and

$$F(V^{\rm ss}, W^{\rm ss}) + \overline{\kappa}(U^{\rm ss}(0) - V^{\rm ss}) = 0, \quad G(V^{\rm ss}, W^{\rm ss}) = 0. \tag{2.5}$$

As in Refs. [21, 22], we will make our analysis more concrete by using the Sel'kov model for which

$$F(V, W) = lW + WV^2 - V, \quad G(V, W) = \epsilon[\mu - (lW + WV^2)]. \tag{2.6}$$

A similar analysis could be carried out for other choices of nonlinear kinetics, such as a Fitzhugh-Nagumo system. The uncoupled system $\dot{V} = F(V, W)$, $\dot{W} = G(V, W)$ then has the unique steady-state $V^* = \mu$, $\quad W^* = \mu/(l + \mu^2)$, and equation (2.5) has the unique solution

$$V^{\rm ss} = \frac{\mu}{1+\overline{\kappa}} + \frac{\overline{\kappa}U^{\rm ss}(0)}{1+\overline{\kappa}}, \quad W^{\rm ss} = \frac{\mu}{l + (V^{\rm ss})^2}. \tag{2.7}$$

Finally, solving for $U^{\rm ss}(x)$ we have

$$U^{\rm ss}(x) = U^* \frac{\cosh(\omega(L-x))}{\cosh(\omega L)}, \quad U^* = \frac{\kappa\mu}{\kappa + D\omega(1+\overline{\kappa})\tanh(\omega L)}, \quad \omega = \sqrt{\frac{\gamma}{D}}. \tag{2.8}$$

2.2. Linearization

In order to analyze the linear stability of the symmetric steady-state solution, we introduce the (stochastic) perturbations

$$u(x,t) = U^{\rm ss}(x) + c(x,t), \quad V_r(t) = V^{\rm ss} + \varphi_r(t), \quad W_r(t) = W^{\rm ss} + \phi_r(t).$$

Substituting into the full system given by equations (2.1) and (2.2), and linearizing about the steady-state solution leads to the following system of linear equations:

$$\frac{\partial c}{\partial t} = D\frac{d^2c}{dx^2} - \gamma c \tag{2.9a}$$

for $x \in [0, 2L]$ with exterior boundary conditions

$$-Dc_x(0,t) = \kappa(\varphi_0(t) - c(0,t)), \quad Dc_x(2L,t) = \kappa(\varphi_1(t) - c(2L,t)), \tag{2.9b}$$

and $n(t)$-dependent boundary conditions on the interior boundary at $x = L$:

$$c(L^-,t) = c(L^+,t), \quad \partial_x c(L^-,t) = \partial_x c(L^+,t) \quad \text{for } n(t) = 0, \tag{2.9c}$$

$$\partial_x c(L^-,t) = 0 = \partial_x c(L^+,t) \quad \text{for } n(t) = 1. \tag{2.9d}$$

Here φ_r, ϕ_r satisfy the equations

$$\frac{d\varphi_r}{dt} = F_V^{\rm ss}\varphi_r + F_W^{\rm ss}\phi_r + \overline{\kappa}[c_r(2Lr,t) - \varphi_r], \tag{2.10a}$$

$$\frac{d\phi_r}{dt} = G_V^{\rm ss}\varphi_r + G_W^{\rm ss}\phi_r \tag{2.10b}$$

for $r = 0, 1$. We have defined $F_V^{\rm ss} = F_V(V^{\rm ss}, W^{\rm ss})$ etc. Note that these linear equations differ in two respects from the corresponding equations of Gou et al [21, 22]. First, they are stochastic due to the presence of a stochastic gate at $x = L$. Second, the presence of the gate means that we cannot impose on the perturbations some form of symmetry condition about the midline.

3. Linear stability analysis of symmetric steady state

We would like to determine the stability of the symmetric steady-state solution in terms of whether or not the linear perturbations $c(x,t), \varphi_r(t), \phi_r(t)$ grow in time. However, we have to deal with the fact that the linearized equations are stochastic. In fact equations (2.9a)–(2.10b) form a piecewise deterministic PDE-ODE system, that is, between switches in the state of the gate at $x = L$, the PDE-ODE system evolves deterministically. This motivates us to introduce the first moments

$$C_n(x,t) = \mathbb{E}[c(x,t)1_{n(t)=n}],\ X_{n,r}(t) = \mathbb{E}[\varphi_r(t)1_{n(t)=n}],\ Y_{n,r}(t) = \mathbb{E}[\phi_r(t)1_{n(t)=n}]. \tag{3.1}$$

We will then investigate a restricted form of stability based on solutions of the resulting first-order moment equations. We derive the latter by extending the recent analysis of 1D diffusion in domains with switching boundaries [27, 3]. In particular, we derive the moment equations by discretizing space and constructing the Chapman-Kolmogorov (CK) equation for the resulting finite-dimensional stochastic hybrid system. (For an alternative method based on probabilistic methods see Ref. [29].) The first step is to spatially discretize the piecewise deterministic PDE (2.9) using a finite-difference scheme. One advantageous feature of this discretization is that the boundary conditions can be incorporated into the resulting discrete Laplacian. Introduce the lattice spacing a such that $(M-1)a = L^-$, $(M+1)a = L^+$ for some integer M. Set $c_j(t) = c(aj,t)$, $j = 0, \ldots, 2M+1$. Then

$$\frac{dc_i}{dt} = \sum_{j=1}^{M-1} \Delta_{ij}^n c_j + \sum_{j=M+1}^{2M} \Delta_{ij}^n c_j + \eta_0 \delta_{i,1} + \eta_1 \delta_{i,N} - \gamma c_i, \tag{3.2}$$

for $i = 1, \ldots, M-1, M+1, \ldots, 2M$ and $n = 0, 1$. The constants η_0, η_1 are determined below. Away from the boundaries ($i \neq 1, M \pm 1, 2M$), Δ_{ij}^n is given by the discrete Laplacian

$$\Delta_{ij}^n = \frac{D}{a^2}[\delta_{i,j+1} + \delta_{i,j-1} - 2\delta_{i,j}]. \tag{3.3}$$

On the left-hand and right-hand exterior boundaries we have

$$-\frac{D}{2a}(c_2 - c_0) = \kappa(\varphi_0 - c_1), \quad \frac{D}{2a}(c_{2M+1} - c_{2M-1}) = \kappa(\varphi_1 - c_{2M}),$$

with $\varphi_{0,1}$ evolving according to the system of ODEs

$$\frac{d\varphi_r}{dt} = F_V^{\rm ss}\varphi_r + F_W^{\rm ss}\phi_r + \overline{\kappa}[c_{[2M-1]i+1}(t) - \varphi_r(t)], \tag{3.4a}$$

$$\frac{d\phi_r}{dt} = G_V^{\rm ss}\varphi_r + G_W^{\rm ss}\phi_r. \tag{3.4b}$$

The exterior boundary conditions can be implemented by taking

$$\Delta_{1j}^n = \frac{D}{a^2}\left[\left(1 + \frac{D}{D+2\kappa a}\right)\delta_{j,2} - 2\delta_{j,1}\right] \tag{3.5a}$$

$$\Delta_{2M,j}^n = \frac{D}{a^2}\left[\left(1 + \frac{D}{D+2\kappa a}\right)\delta_{j,2M-1} - 2\delta_{j,2M}\right], \tag{3.5b}$$

and

$$\eta_0 = \frac{D}{a^2}\frac{2\kappa a}{D+2\kappa a}\varphi_0, \quad \eta_1 = \frac{D}{a^2}\frac{2\kappa a}{D+2\kappa a}\varphi_1. \tag{3.5c}$$

On the interior boundary,

$$c_{M-2} - c_M^- = c_M^+ - c_{M+2}, \quad c_M^+ = c_M^-, \quad \text{if } n = 0,$$

and

$$c_{M-2} - c_M^- = 0, \quad c_{M+2} - c_M^+ = 0, \quad \text{if } n = 1.$$

(Recall that we are taking c_M^- to be c_{M-1} and c_M^+ to be c_{M+1}.) These can be implemented by taking

$$\Delta_{1j}^n = \frac{D}{a^2}[\delta_{j,2} - 2\delta_{j,1}], \quad \Delta_{Qj}^n = \frac{D}{a^2}[\delta_{Q-1,j} - 2\delta_{Q,j}], \quad n = 0, 1, \tag{3.6a}$$

$$\Delta_{M-1,j}^0 = \frac{D}{a^2}[\delta_{M-2,j} + (\delta_{M-2,j} + \delta_{M+2,j})/2 - 2\delta_{M-1,j}], \tag{3.6b}$$

$$\Delta_{M+1,j}^0 = \frac{D}{a^2}[\delta_{M+2,j} + (\delta_{M-2,j} + \delta_{M+2,j})/2 - 2\delta_{M+1,j}], \tag{3.6c}$$

and

$$\Delta_{M\pm1,j}^1 = \frac{2D}{a^2}[\delta_{M\pm2,j} - \delta_{M\pm1,j}]. \tag{3.6d}$$

Note that when $n = 1$ the system of equations in the two compartments decouple (as expected for a closed gate).

Our spatial discretization scheme has reduced the system to a piecewise deterministic ODE known as a stochastic hybrid system [2]. Let

$$\mathbf{c}(t) = (c_1(t), \ldots, c_{M-1}(t), c_{M+1}(t), \ldots, c_{2M}(t)),\ \mathbf{X}(t) = (\varphi_0(t), \varphi_1(t), \phi_0(t), \phi_1(t))$$

and introduce the probability density

$$\text{Prob}\{\mathbf{c}(t) \in (\mathbf{c}, \mathbf{c}+d\mathbf{c}), \mathbf{X}(t) \in (\mathbf{X}, \mathbf{X}+d\mathbf{X}, n(t) = n\} = p_n(\mathbf{c}, \mathbf{X}, t)d\mathbf{c}\, d\mathbf{X}, \tag{3.7}$$

where we have dropped the explicit dependence on initial conditions. The probability density evolves according to the differential Chapman-Kolmogorov (CK) equation [18, 2]

$$\begin{aligned}
\frac{\partial p_n}{\partial t} &= -\sum_{i=1}^{2M} \frac{\partial}{\partial c_i}\left[\left(\sum_{j=1, j\neq M}^{2M} \Delta_{ij}^n c_j - \gamma c_i + \eta_0\delta_{i,1} + \eta_1\delta_{i,2M}\right) p_n\right] \\
&\quad - \sum_{r=0,1} \frac{\partial}{\partial \varphi_r}\left[\left(F_V^{\text{ss}}\varphi_r + F_W^{\text{ss}}\phi_r + \overline{\kappa}[c_{(2M-1)r+1} - \varphi_r]\right) p_n\right] \\
&\quad - \sum_{r=0,1} \frac{\partial}{\partial \phi_r}\left[\left(G_V^{\text{ss}}\varphi_r + G_W^{\text{ss}}\phi_r\right) p_n\right] + \sum_{m=0,1} A_{nm}p_m,
\end{aligned} \tag{3.8}$$

where A is the matrix

$$A = \begin{bmatrix} -\beta & \alpha \\ \beta & -\alpha \end{bmatrix}. \tag{3.9}$$

The right-hand side consists of an advection term representing the deterministic evolution of the system in between jumps of the discrete variable, with the latter

represented by the matrix A. (The transpose $A^\top$ is the generator of the Markov process.) The left nullspace of A is spanned by the vector

$$\psi = \begin{pmatrix} 1 \\ 1 \end{pmatrix}, \tag{3.10}$$

and the right nullspace is spanned by

$$\rho \equiv \begin{pmatrix} \rho_0 \\ \rho_1 \end{pmatrix} = \frac{1}{\alpha+\beta} \begin{pmatrix} \alpha \\ \beta \end{pmatrix}. \tag{3.11}$$

A simple application of the Perron-Frobenius theorem shows that the two state Markov process with master equation

$$\frac{dP_n(t)}{\partial t} = \sum_{m=0,1} A_{nm} P_m(t) \tag{3.12}$$

is ergodic with $\lim_{t\to\infty} P_n(t) = \rho_n$.

Having derived the CK equation for the spatially discretized system, we can now derive equations for the first-order moments

$$C_{n,k}(t) = \mathbb{E}[c_k(t) 1_{n(t)=n}] = \int p_n(\mathbf{c}, \mathbf{X}, t) c_k(t) d\mathbf{c}\, d\mathbf{X}, \tag{3.13}$$

$$X_{n,r}(t) = \mathbb{E}[\varphi_r(t) 1_{n(t)=n}] = \int p_n(\mathbf{c}, \mathbf{X}, t) \varphi_r(t) d\mathbf{c}\, d\mathbf{X}, \quad r = 0, 1, \tag{3.14}$$

and

$$Y_{n,r}(t) = \mathbb{E}[\phi_r(t) 1_{n(t)=n}] = \int p_n(\mathbf{c}, \mathbf{X}, t) \phi_r(t) d\mathbf{c}\, d\mathbf{X}, \quad r = 0, 1. \tag{3.15}$$

First, multiplying both sides of the CK equation (3.8) by $c_k(t)$ and integrating with respect to $\mathbf{c}, \mathbf{X}$ gives (after integration by parts)

$$\begin{aligned} \frac{dC_{n,k}}{dt} &= \sum_{j=1, j\neq M}^{2M} \Delta^n_{kj} C_{n,j} - \gamma C_{n,k} + \mathbb{E}[\eta_0(t) 1_{n(t)=n}] \delta_{i,1} + \mathbb{E}[\eta_1(t) 1_{n(t)=n}] \delta_{i,2M} \\ &\quad + \sum_{m=0,1} A_{nm} C_{m,k}. \end{aligned}$$

with $\eta_{0,1}$ defined by equations (3.5c). Similarly, multiplying both sides of the CK equation (3.8) by $\varphi_r(t)$ and integrating with respect to $\mathbf{c}, \mathbf{X}$ gives (after integration by parts)

$$\begin{aligned} \frac{dX_{n,r}}{dt} &= F^{\text{ss}}_V X_{n,r} + F^{\text{ss}}_W Y_{n,r} + \overline{\kappa}[C_{n,(2M-1)r+1} - X_{n,r}], \\ \frac{dY_{n,r}}{dt} &= G^{\text{ss}}_V X_{n,r} + G^{\text{ss}}_W Y_{n,r}, \quad r = 0, 1. \end{aligned}$$

If we now take the continuum limit, $a \to 0, M \to \infty$ such that $aM = L$, then we obtain the system of equations for the first-order moments (3.1)

$$\frac{\partial C_0}{\partial t} = D\frac{\partial^2 C_0}{\partial x^2} - \gamma C_0 - \beta C_0 + \alpha C_1 \tag{3.16a}$$

$$\frac{\partial C_1}{\partial t} = D\frac{\partial^2 C_1}{\partial x^2} - \gamma C_1 + \beta C_0 - \alpha C_1 \tag{3.16b}$$

for $x \in [0, 2L]$ with exterior boundary conditions

$$-D\partial_x C_n(0,t) = \kappa(X_{n,0}(t) - C_n(0,t)),\ D\partial_x C_n(2L,t) = \kappa(X_{n,1}(t) - C_n(2L,t)), \tag{3.16c}$$

and interior boundary conditions

$$\begin{aligned} C_0(L^-,t) &= C_0(L^+,t),\ \partial_x C_0(L^-,t) = \partial_x C_0(L^+,t), \\ \partial_x C_1(L^-,t) &= 0 = \partial_x C_1(L^+,t). \end{aligned} \tag{3.16d}$$

Moreover,

$$\frac{dX_{n,r}}{dt} = F_V^{\rm ss} X_{n,r} + F_W^{\rm ss} Y_{n,r} + \overline{\kappa}[C_n(2Lr,t) - X_{n,r}], \tag{3.17a}$$

$$\frac{dY_{n,r}}{dt} = G_V^{\rm ss} X_{n,r} + G_W^{\rm ss} Y_{n,r}, \quad r = 0,1, \quad n = 0,1. \tag{3.17b}$$

We note that these first-order moment equations and boundary conditions, (3.16a)-(3.17b), can be obtained through a separate argument using probabilistic methods [29].

3.1. Spectral problem

In order to investigate stability of the steady-state solution with respect to first-order moments of the perturbations, we take

$$C_n(x,t) = \mathrm{e}^{\lambda t} C_n(x), \quad X_{n,r}(t) = \mathrm{e}^{\lambda t} X_{n,r}, \quad Y_{n,r}(t) = \mathrm{e}^{\lambda t} Y_{n,r}. \tag{3.18}$$

We then obtain the following system of time-independent equations:

$$\lambda C_0 = D\frac{d^2 C_0}{dx^2} - \gamma C_0 - \beta C_0 + \alpha C_1 \tag{3.19a}$$

$$\lambda C_1 = D\frac{d^2 C_1}{dx^2} - \gamma C_1 + \beta C_0 - \alpha C_1 \tag{3.19b}$$

for $x \in [0, 2L]$ with exterior boundary conditions

$$-D\partial_x C_n(0) = \kappa(X_{n,0} - C_n(0)),\ D\partial_x C_n(2L) = \kappa(X_{n,1} - C_n(2L)), \tag{3.19c}$$

and interior boundary conditions

$$C_0(L^-) = C_0(L^+),\ \partial_x C_0(L^-) = \partial_x C_0(L^+),\ \partial_x C_1(L^-) = 0 = \partial_x C_1(L^+). \tag{3.19d}$$

Moreover,

$$\lambda X_{n,r} = F_V^{\rm ss} X_{n,r} + F_W^{\rm ss} Y_{n,r} + \overline{\kappa}[C_n(2Lr) - X_{n,r}], \tag{3.20a}$$
$$\lambda Y_{n,r} = G_V^{\rm ss} X_{n,r} + G_W^{\rm ss} Y_{n,r}, \quad r = 0, 1, \quad n = 0, 1. \tag{3.20b}$$

From the interior boundary conditions (3.19d), we set

$$-D\partial_x C_0(L^-) = -D\partial_x C_0(L^+) = J_0,$$

with J_0 to be determined later by imposing $C_0(L^-) = C_0(L^+)$. Adding equations (3.19a) and (3.19b) then gives

$$D\frac{d^2C}{dx^2} - (\gamma + \lambda)C = 0, \quad x \in [0, L), \tag{3.21a}$$
$$-D\partial_x C(0) = \kappa(X_0 - C(0)), \quad -D\partial_x C(L^-) = J_0, \tag{3.21b}$$

and

$$\frac{d^2C}{dx^2} - (\gamma + \lambda)C = 0, \quad x \in (L, 2L], \tag{3.22a}$$
$$-D\partial_x C(L^+) = J_0,\ D\partial_x C(2L) = \kappa(X_1 - C(2L)). \tag{3.22b}$$

We have set

$$C(x) = C_0(x) + C_1(x), \quad X_r = X_{0,r} + X_{1,r},$$

so that $C(x)$ is the mean cytosolic concentration and X_r is the mean concentration at the end $r = 1, 2$ irrespective of the state of the gate. We obtain the piecewise solution

$$C(x) = \begin{cases} C^-(x) & x \in [0, L) \\ C^+(x) & x \in (L, 2L] \end{cases} \tag{3.23a}$$

with

$$C^-(x) = \frac{\kappa(X_0 + J_0(\lambda))}{\kappa + D\omega_\lambda \tanh(\omega_\lambda L)} \frac{\cosh(\omega_\lambda(L - x))}{\cosh(\omega_\lambda L)} - J_0(\lambda)\cosh(\omega_\lambda x), \tag{3.23b}$$

and

$$C^+(x) = \frac{\kappa(X_1 - J_0(\lambda))}{\kappa + D\omega_\lambda \tanh(\omega_\lambda L)} \frac{\cosh(\omega_\lambda(L - x))}{\cosh(\omega_\lambda L)} + J_0(\lambda)\cosh(\omega_\lambda(2L - x)). \tag{3.23c}$$

Here

$$J_0(\lambda) = \frac{J_0}{D\omega_\lambda \sinh(\omega_\lambda L)}, \quad \omega_\lambda = \sqrt{\frac{\lambda + \gamma}{D}}. \tag{3.24}$$

We note that we need the principal branch for ω_λ, which has a branch cut on portions of the negative real axis as a function of λ.

Since $C_0 = C - C_1$, we can rewrite equation (3.19b) as

$$D\frac{d^2C_1}{dx^2} - (\alpha+\beta+\gamma+\lambda)C_1(x) = -\beta C(x) \tag{3.25}$$

with

$$-D\partial_x C_1(0) = \kappa(X_{1,0} - C_1(0)), \quad D\partial_x C_1(2L) = \kappa(X_{1,1} - C_1(2L)),$$

and

$$\partial_x C_1(L^-) = 0 = \partial_x C_1(L^+).$$

Substituting for $C(x)$ using equation (3.23a) we obtain a piecewise solution of the form

$$C_1(x) = \begin{cases} C_1^-(x) & x \in [0, L) \\ C_1^+(x) & x \in (L, 2L] \end{cases} \tag{3.26a}$$

with

$$C_1^-(x) = \rho_1 C^-(x) + \frac{\kappa\left[X_{1,0} - \rho_1 X_0 - \mathcal{A}\right]}{\kappa + D\Omega_\lambda \tanh(\Omega_\lambda L)} \frac{\cosh(\Omega_\lambda(L-x))}{\cosh(\Omega_\lambda L)} + \mathcal{A}\cosh(\Omega_\lambda x), \tag{3.26b}$$

$$C_1^+(x) = \rho_1 C^+(x) + \frac{\kappa\left[X_{1,1} - \rho_1 X_1 - \mathcal{B}\right]}{\kappa + D\Omega_\lambda \tanh(\Omega_\lambda L)} \frac{\cosh(\Omega_\lambda(L-x))}{\cosh(\Omega_\lambda L)} + \mathcal{B}\cosh(\Omega_\lambda[2L-x]) \tag{3.26c}$$

with

$$\Omega_\lambda = \sqrt{\frac{\lambda+\gamma+\alpha+\beta}{D}}.$$

As above, we need the principal branch for Ω_λ, which has a branch cut on portions of the negative real axis as a function of λ. We have imposed the exterior boundary conditions. The interior boundary conditions for C_1 then determine the coefficients $\mathcal{A}, \mathcal{B}$ in terms of J_0:

$$\mathcal{A} = \frac{\rho_1 J_0}{D\Omega_\lambda \sinh(\Omega_\lambda L)} = -\mathcal{B}. \tag{3.27}$$

Finally, we determine the unknown J_0 by requiring that $C_0(x)$ is continuous across $x = L$. However, we will not need the explicit expression for J_0.

Next we write equations (3.20a) and (3.20b) in the matrix form

$$(\mathbf{J} - \lambda\mathbf{I}) \begin{pmatrix} X_{n,r} \\ Y_{n,r} \end{pmatrix} = \overline{\kappa}\left[X_{n,r} - C_n(2Lr)\right] \begin{pmatrix} 1 \\ 0 \end{pmatrix},$$

where

$$\mathbf{J} = \begin{pmatrix} F_V^{\rm ss} & F_W^{\rm ss} \\ G_V^{\rm ss} & G_W^{\rm ss} \end{pmatrix}. \tag{3.28}$$

Using the fact that the first entry of the vector $(\mathbf{J} - \lambda\mathbf{I}) \begin{pmatrix} 1 \\ 0 \end{pmatrix}$ is

$$(\mathbf{J} - \lambda\mathbf{I})^{-1} \begin{pmatrix} 1 \\ 0 \end{pmatrix}\Big|_1 = \Theta(\lambda) \equiv \frac{G_W^{\rm ss} - \lambda}{\det[\mathbf{J} - \lambda\mathbf{I}]},$$

we obtain the system of self-consistency conditions

$$X_{n,r} = \overline{\kappa}\Theta(\lambda)\left[X_{n,r} - C_n(2Lr)\right], \quad n, r = 0, 1. \tag{3.29}$$

We thus expect to obtain four branches of solutions for λ, in contrast to the single branch obtained by Gou et al [21, 22] (our additional branches stem from the stochastic gate). Summing equation (3.29) with respect to r and setting $S_n = X_{n,0} + X_{n,1}$ yields the pair of closed equations

$$S_0 = \overline{\kappa}\Theta(\lambda)[S_0 - C_0(0) - C_0(2L)], \quad S_1 = \overline{\kappa}\Theta(\lambda)[S_1 - C_1(0) - C_1(2L)].$$

Substituting for $C_n(0) + C_n(2L)$ using equations (3.23) and (3.26), and noting that all terms involving J_0 cancel, we find that

$$S_0 = \overline{\kappa}\Theta(\lambda)[S_0 - \rho_0\Gamma(\omega_\lambda)S + \Gamma(\Omega_\lambda)(S_1 - \rho_1 S)], \tag{3.30a}$$
$$S_1 = \overline{\kappa}\Theta(\lambda)[S_1 - \rho_1\Gamma(\omega_\lambda)S - \Gamma(\Omega_\lambda)(S_1 - \rho_1 S)], \tag{3.30b}$$

where

$$\Gamma(\omega) = \frac{\kappa}{\kappa + D\omega\tanh(\omega L)}.$$

Here $S = X_0 + X_1 = \overline{X}_0 + \overline{X}_1$. This pair of equations can be decoupled by considering the linear combinations $S = S_0 + S_1$ and $\widehat{S} = \rho_1 S_0 - \rho_0 S_1$ to yield the following characteristic equations for λ:

$$\left(1 - \overline{\kappa}\Theta(\lambda)[1 - \Gamma(\omega_\lambda)]\right) S = 0, \tag{3.31a}$$
$$\left(1 - \overline{\kappa}\Theta(\lambda)[1 - \Gamma(\Omega_\lambda)]\right) \widehat{S} = 0. \tag{3.31b}$$

In order to obtain the other pair of closed equations, introduce the new variables

$$T_n = X_{n,0} - X_{n,1} \implies X_0 - X_1 = T_0 + T_1 \equiv T,$$

For each $n = 0, 1$ subtract the pair of equations in (3.29) corresponding to $r = 0, 1$. this yields

$$T_0 = \overline{\kappa}\Theta(\lambda)[T_0 - C_0(0) + C_0(2L)], \quad T_1 = \overline{\kappa}\Theta(\lambda)[T_1 - C_1(0) + C_1(2L)].$$

Substituting for $C_n(0) - C_n(2L)$ using equations (3.23) and (3.26) gives

$$\begin{aligned} T_0 = \overline{\kappa}\Theta(\lambda)\Big[&T_0 - (\rho_0\Gamma(\omega_\lambda) + \rho_1\Gamma(\Omega_\lambda))T + \Gamma(\Omega_\lambda)T_1 \\ &+ 2(1 - \Gamma(\Omega_\lambda))\mathcal{A} + 2\rho_0(1 - \Gamma(\omega_\lambda))J_0(\lambda)\Big], \\ T_1 = \overline{\kappa}\Theta(\lambda)\Big[&T_1 - (\rho_1\Gamma(\omega_\lambda) - \rho_1\Gamma(\Omega_\lambda))T - \Gamma(\Omega_\lambda)T_1 \\ &- 2(1 - \Gamma(\Omega_\lambda))\mathcal{A} + 2\rho_1(1 - \Gamma(\omega_\lambda))J_0(\lambda)\Big]. \end{aligned}$$

This pair of equations can be rewritten in terms of the linear combinations $T = T_0 + T_1$ and $\widehat{T} = \rho_1 T_0 - \rho_0 T_1$ as follows:

$$\begin{aligned} T &= \overline{\kappa}\Theta(\lambda)[1 - \Gamma(\omega_\lambda)](T + 2J_0(\lambda)) \\ \widehat{T} &= \overline{\kappa}\Theta(\lambda)[1 - \Gamma(\Omega_\lambda)](\widehat{T} + 2\mathcal{A}). \end{aligned} \tag{3.32}$$

Note that $J_0(\lambda)$ and $\mathcal{A}$ both depend on J_0 which in turn depends on T and $\widehat{T}$. In particular, by setting $C_0(L^-) = C_0(L^+)$ and using equations (3.26) and (3.23), we can solve for J_0 which allows us to obtain

$$2J_0(\lambda) = \xi_\lambda\big[q_\lambda^{11}T + q_\lambda^{12}\widehat{T}\big] \quad \text{and} \quad 2\mathcal{A} = \xi_\lambda\big[q_\lambda^{21}T + q_\lambda^{22}\widehat{T}\big],$$

where

$$\begin{aligned}\frac{1}{\xi_\lambda} &= \rho_0\Omega_\lambda\coth(\omega_\lambda L) + \rho_1\omega_\lambda\coth(\Omega_\lambda L)\\ &\quad - 2\rho_0\Omega_\lambda\Gamma(\omega_\lambda)\mathrm{csch}(2\omega_\lambda L) - 2\rho_1\omega_\lambda\Gamma(\Omega_\lambda)\mathrm{csch}(2\Omega_\lambda L),\end{aligned}$$

and

$$\begin{aligned}q_\lambda^{11} &= 2\rho_0\Omega_\lambda\Gamma(\omega_\lambda)\mathrm{csch}(2\omega_\lambda L), & q_\lambda^{12} &= \Omega_\lambda\Gamma(\Omega_\lambda)\mathrm{csch}(\omega_\lambda L)\mathrm{sech}(\Omega_\lambda L)\\ q_\lambda^{21} &= \rho_0\rho_1\omega_\lambda\Gamma(\omega_\lambda)\mathrm{csch}(\Omega_\lambda L)\mathrm{sech}(\omega_\lambda L), & q_\lambda^{22} &= 2\rho_1\omega_\lambda\Gamma(\Omega_\lambda)\mathrm{csch}(2\Omega_\lambda L)\end{aligned}$$

Equations (3.31) and (3.32) can now be used to investigate conditions on λ with respect to excitation of different eigenmodes corresponding to different linear combinations of $X_{n,r}$, $n, r = 0, 1$.

1. **In-phase mode**: For $S \neq 0, \widehat{S} = T = \widehat{T} = 0$ we have the in-phase state $X_0 = X_1$ where the two ends are symmetric for both $n = 0, 1$, that is,

   $$X_{0,0} = X_{0,1}, \quad X_{1,0} = X_{1,1}.$$

   The corresponding spectral condition is

   $$1 - \overline{\kappa}\Theta(\lambda)[1 - \Gamma(\omega_\lambda)] = 0,$$

   which, on rearranging yields the equation

   $$\mathcal{F}^s(\lambda) \equiv \frac{1}{s(\lambda)} - \frac{G_W^{\mathrm{ss}} - \lambda}{\det[\mathbf{J} - \lambda\mathbf{I}]} = 0, \tag{3.33a}$$

   with

   $$s(\lambda) = \frac{\overline{\kappa}D\omega_\lambda\tanh(\omega_\lambda L)}{\kappa + D\omega_\lambda\tanh(\omega_\lambda L)}. \tag{3.33b}$$

2. **Null-mode**: For $\widehat{S} \neq 0, S = T = \widehat{T} = 0$ we have the null mode $X_0 = X_1 = 0$ with

   $$X_{0,0} = -X_{1,0} = -X_{1,1} = X_{0,1} \neq 0.$$

   We now have

   $$1 - \overline{\kappa}\Theta(\lambda)[1 - \Gamma(\Omega_\lambda)] = 0,$$

   which, on rearranging yields the equation

   $$\widehat{\mathcal{F}}^s(\lambda) \equiv \frac{1}{\widehat{s}(\lambda)} - \frac{G_W^{\mathrm{ss}} - \lambda}{\det[\mathbf{J} - \lambda\mathbf{I}]} = 0, \tag{3.34a}$$

   with

   $$\widehat{s}(\lambda) = \frac{\overline{\kappa}D\Omega_\lambda\tanh(\Omega_\lambda L)}{\kappa + D\Omega_\lambda\tanh(\Omega_\lambda L)}. \tag{3.34b}$$

3. **Anti-phase mixed modes**: For $\widehat{S} = S = 0$ we have an anti-phase state $X_0 = -X_1$ with the additional condition that

$$X_{0,0} + X_{0,1} = \frac{\rho_0}{\rho_1}(X_{1.0} + X_{1,1}).$$

The conditions (3.32) can be written in the form

$$\begin{aligned} T &= \overline{\kappa}\Theta(\lambda)\big[1 - \Gamma(\omega_\lambda)\big]\Big((1 + \xi_\lambda q_\lambda^{11})T + \xi_\lambda q_\lambda^{12}\widehat{T}\Big) \\ \widehat{T} &= \overline{\kappa}\Theta(\lambda)\big[1 - \Gamma(\Omega_\lambda)\big]\Big(\xi_\lambda q_\lambda^{21}T + (1 + \xi_\lambda q_\lambda^{22})\widehat{T}\Big). \end{aligned}$$

We note that $T \neq 0$ if and only if $\widehat{T} \neq 0$. Importantly, we also note that in the fast switching limit we have $\widehat{T} \to 0$, and the condition for T recovers the spectrum obtained by Gou et al [21, 22] in the absence of a gate and for anti-phase perturbations. To see this, we fix ρ_0 and take $\alpha + \beta \to \infty$ (and thus $\Omega_\lambda \to \infty$) to obtain

$$\begin{aligned} \lim_{\Omega_\lambda \to \infty} \xi_\lambda q_\lambda^{ij} &= 0, \quad \text{for } i \neq 1 \text{ or } j \neq 1, \\ \lim_{\Omega_\lambda \to \infty} \xi_\lambda q_\lambda^{11} &= \frac{2\kappa\,\mathrm{csch}(2\omega_\lambda L)}{D\omega_\lambda + \kappa\tanh(\omega_\lambda L)}. \end{aligned} \tag{3.35}$$

Then,

$$\big[1 - \Gamma(\omega_\lambda)\big]\Big(1 + \frac{2\kappa\,\mathrm{csch}(2\omega_\lambda L)}{D\omega_\lambda + \kappa\tanh(\omega_\lambda L)}\Big) = 1 - \frac{\kappa}{\kappa + D\omega_\lambda\coth(\omega_\lambda L)}, \tag{3.36}$$

which, upon plugging into the T equation above, yields the spectrum obtained by Gou et al [21, 22] in the absence of a gate for anti-phase perturbations.

For finite switching rates, we will have two anti-phase modes in which the relationship between the open and closed states at each end is determined by $S = \widehat{S} = 0$ and the solutions, T and $\widehat{T}$, of the equation

$$\left[\begin{pmatrix} \chi_1(\lambda) & 0 \\ 0 & \chi_2(\lambda) \end{pmatrix}(\xi_\lambda Q(\lambda) + I) - I\right]\begin{pmatrix} T \\ \widehat{T} \end{pmatrix} = 0, \tag{3.37}$$

where

$$\chi_1(\lambda) = \overline{\kappa}\Theta(\lambda)\big[1 - \Gamma(\omega_\lambda)\big], \quad \chi_2(\lambda) = \overline{\kappa}\Theta(\lambda)\big[1 - \Gamma(\Omega_\lambda)\big], \tag{3.38}$$

$Q_{ij}(\lambda) = q_\lambda^{ij}$, and I is the identity matrix.

3.2. Winding number analysis

We now investigate equation (3.37) to determine the parameter regimes in which the nonlinear stochastic PDE-ODE system in (2.1) supports stochastic anti-phase oscillations (case 3 above). We focus on this case of anti-phase oscillations because the perturbations in cases 1 and 2 are symmetric about the midline, $x = L$, and are therefore unaffected by the stochastic gate.

Equation (3.37) has a nontrivial solution, T and $\widehat{T}$, if and only if the corresponding determinant is zero:

$$\begin{aligned}\mathcal{G}(\lambda) := &\left[\chi_1(\lambda)\xi_\lambda q_\lambda^{11} + \chi_1(\lambda) - 1\right]\left[\chi_2(\lambda)\xi_\lambda q_\lambda^{22} + \chi_2(\lambda) - 1\right] \\ &- (\xi_\lambda)^2\chi_1(\lambda)\chi_2(\lambda)q_\lambda^{12}q_\lambda^{21}.\end{aligned} \tag{3.39}$$

Following [24], we determine the number of roots of $\mathcal{G}(\lambda)$ in $\mathrm{Re}(\lambda) > 0$ using the argument principle of complex analysis. To do this, we compute the winding number of $\mathcal{G}(\lambda)$ over the contour consisting of the semi-circle, $|\lambda| = R$, with $\mathrm{Re}(\lambda) > 0$, denoted by Γ_R, and the imaginary axis, $\Gamma_+ \cup \Gamma_-$, where $\Gamma_+ = i\lambda_I$ and $\Gamma_- = -i\lambda_I$ for $0 \le \lambda_I \le R$. Assuming there are no pure imaginary roots of $\mathcal{G}(\lambda) = 0$, we have by the argument principle that the number of roots, N, of $\mathcal{G}(\lambda)$ in $\mathrm{Re}(\lambda) > 0$ is

$$N = \frac{1}{2\pi}\Big(\lim_{R\to\infty}[\arg\,\mathcal{G}]_{\Gamma_R} + \lim_{R\to\infty}[\arg\,\mathcal{G}]_{\Gamma_+} + \lim_{R\to\infty}[\arg\,\mathcal{G}]_{\Gamma_-}\Big) + P,$$

where $[\arg\,\mathcal{G}]_\Gamma$ denotes the change in the argument of $\mathcal{G}$ over the contour Γ oriented in the counterclockwise direction, and P is the number of poles of $\mathcal{G}(\lambda)$ in $\mathrm{Re}(\lambda) > 0$ counted according to their multiplicity.

It is straightforward to check that the only poles of $\mathcal{G}(\lambda)$ in $\mathrm{Re}(\lambda) > 0$ occur in the $\chi_1(\lambda)$ and $\chi_2(\lambda)$ terms when $\Theta(\lambda)$ has a pole because $\det[\mathbf{J} - \lambda\mathbf{I}] = 0$. By the particular form of $\mathbf{J}$, we see that $\Theta(\lambda)$ has 2 poles in $\mathrm{Re}(\lambda) > 0$ if the trace of $\mathbf{J}$ is positive and 0 poles if the trace of $\mathbf{J}$ is negative. Since $\mathcal{G}$ contains products of χ_1 and χ_2 and poles are counted by multiplicity, we have that

$$P = \begin{cases} 0, & \text{if } \mathrm{tr}(\mathbf{J}) < 0, \\ 4, & \text{if } \mathrm{tr}(\mathbf{J}) > 0. \end{cases} \tag{3.40}$$

Next, it is straightforward to check that

$$\lim_{|\lambda|\to\infty} \mathcal{G}(\lambda) = 1, \quad \text{if } \mathrm{Re}(\lambda) \ge 0.$$

Thus, $\lim_{R\to\infty}[\arg\,\mathcal{G}]_{\Gamma_R} = 0$. Furthermore, $\overline{\mathcal{G}(\lambda)} = \mathcal{G}(\overline{\lambda})$, and thus $[\arg\,\mathcal{G}]_{\Gamma_+} = [\arg\,\mathcal{G}]_{\Gamma_-}$. Therefore, in order to find N it remains only to calculate $\lim_{R\to\infty}[\arg\,\mathcal{G}]_{\Gamma_+}$. Since $\mathcal{G}(0) > 0$ and $\lim_{R\to\infty}\mathcal{G}(iR) = 1 > 0$, the change in the argument of $\mathcal{G}$ over Γ_+ can only be an integer multiple of 2π. Putting this together, we conclude that

$$N = 2m + P,$$

where m is the winding number of $\mathcal{G}$ over the contour Γ_+, and P is given by (3.40).

The winding number, m, can be calculated numerically from equation (3.39). This is illustrated in Fig. 3, where we plot in the complex plane the path of $\mathcal{G}(iR)$ as R ranges from a large positive value to zero for two particular parameter sets. For one of the parameter sets ($D = 0.65$ and $\overline{\kappa} = 0.5$), the curve $(\mathrm{Re}\,(\mathcal{G}(iR)), \mathrm{Im}\,(\mathcal{G}(iR)))$ wraps around the origin once in the complex plane in the clockwise direction. Hence, $m = -1$. For this parameter set, $\mathrm{tr}(\mathbf{J}) > 0$, so $P = 4$, and thus $N = 2$. We note that plotting $\mathcal{G}(R)$ for a large range of positive R values allows one to check that $\mathcal{G}(R) > 0$ for $R > 0$, and thus the roots of $\mathcal{G}(\lambda)$ in $\mathrm{Re}(\lambda) > 0$ are complex, and hence the corresponding instability of (2.1) is oscillatory. For the other parameter set considered in Fig. 3, $m = -2$, $P = 4$, and thus $N = 0$.

3.3. Phase diagrams and stochastic simulations of the full system

By computing the m and P for different parameter values, we can determine the parameter curves along which the first-moment equations (3.16a)-(3.17b) undergo a Hopf bifurcation. However, linear stability analysis alone cannot establish whether or not a Hopf bifurcation is supercritical, that is, whether or not the emerging limit cycle is stable. The analysis is further complicated by the fact that, as in the ungated system [21, 22], the Hopf curves for in-phase and anti-phase solutions can intersect, resulting in a change of stability of in-phase or anti-phase solutions due to the existence of a torus bifurcation. The Hopf curves thus determine regions where limit cycles are expected to occur but their

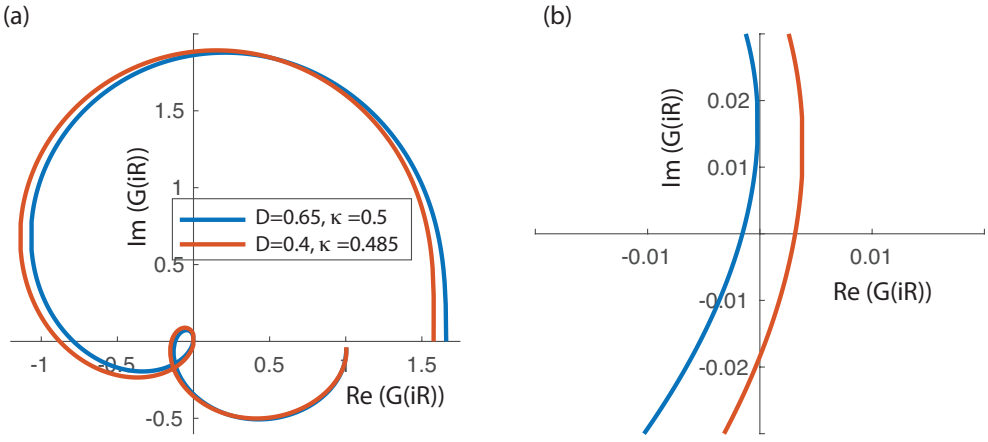

Figure 3: Path of $(\mathrm{Re}\,(\mathcal{G}(iR)), \mathrm{Im}\,(\mathcal{G}(iR)))$ in the complex plane as R ranges from a large positive value to zero. (a) From the left plot, we see that both curves wrap around the origin at least once. (b) Zooming in, the right plot shows that the blue curve wraps around the origin once, and the red curve wraps around the origin twice. For the blue curve, $D = 0.65$ and $\overline{\kappa} = 0.4$, and for the red curve, $D = 0.4$ and $\overline{\kappa} = 0.485$. For both the red and the blue curve, $\alpha = 1$, $\beta = 10$, $\mu = 2$, $l = 0.9$, $\varepsilon = 0.15$, and $\kappa = \gamma = L = 1$.

stability has to be checked numerically. One additional note of caution is that we are considering bifurcations of the symmetric steady state with respect to perturbations that are averaged with respect to realizations of the stochastic gate. Since we find numerically that higher-order fluctuations are unimportant for the given system, we will assume that the existence regions for oscillatory solutions of the first-moment equations also hold for the full stochastic system given by equations (2.1) and (2.2). We check this explicitly below.

Fig. 4 plots phase diagrams for several choices of the switching rates, α and β, of the stochastic gate and compares them to the phase diagrams obtained by Gou et al. in [24] for the ungated system. As noted before, the stochastic gate is irrelevant for in-phase oscillations (and thus the region of parameter space supporting in-phase oscillations is unchanged by the stochastic gate). However, for anti-phase oscillations we see that the stochastic gate alters the phase diagram. There are several interesting regimes of the switching rates to consider. In the following, we refer to the region of parameter space for which a system supports anti-phase (or in-phase) oscillations as the anti-phase (or in-phase) region.

First, if $\alpha/\beta \gg 1$, then the gate is open most of the time. As expected, in this limit the anti-phase region of the gated system in (2.1) approaches the anti-phase region of the ungated system considered in [22] (see the orange curve in Fig. 4). Similarly, for any fixed ratio α/β, the anti-phase region of the gated system approaches the anti-phase region of the ungated system if we take $\alpha+\beta$ sufficiently large (see the blue curve in Fig. 4). That is, even if the gate is closed most of the time (α/β small), the gate essentially has no effect if it opens and closes at sufficiently high frequency (which agrees with our analysis in equations (3.35)-(3.36)). This phenomenon has been explored in several other works (see [27, 3, 28, 7, 29, 30]), and there are multiple ways to understand it. Perhaps the simplest explanation follows from the behavior of a Brownian particle at fine spatial scales; namely, any time a Brownian particle hits a boundary, it hits it infinitely often. Thus, even if the gate is closed when a particle hits it, the particle will hit the gate many times shortly after the first hit, and the gate must be open at one of those times if it's opening and closing at a sufficiently high frequency. Indeed, if a Brownian particle starts on a boundary that switches between reflecting and absorbing, then the mean absorption time vanishes as the switching rate increases [5, 6].

Next, if $\alpha/\beta \ll 1$ for fixed $\alpha+\beta$, then the gate is closed most of the time and the *anti-phase* region of the gated system approaches the *in-phase* region of the ungated system (see the green curve in Fig. 4). The reason for this is the following. From the perspective of the solution restricted to $[0, L]$ (or $[L, 2L]$), a closed gate at $x = L$ is equivalent to a solution that is symmetric about $x = L$. Hence, the system with a gate that is (almost) always closed will support anti-phase oscillations (or oscillations with any given phase relationship) if the ungated system supports in-phase oscillations.

Finally, the most interesting regime is that of intermediate values of the switching rates, α and β (see the red curve in Fig. 4). In this non limiting case, the gated system exhibits behavior not seen in the ungated system. Indeed, there exists parameter regimes where the gated system exhibits oscillations, but

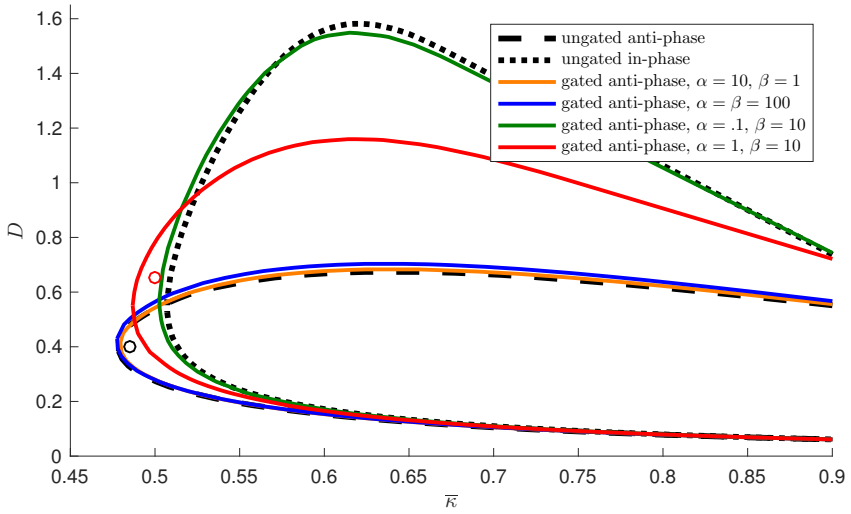

Figure 4: Phase diagram in the $(D, \overline{\kappa})$ plane for the ungated system and several choices of the switching rates of the stochastically gated system. Other parameters are given in the caption of Fig. 3. The black dashed (respectively, dotted) curve encloses the set of $(D, \overline{\kappa})$ values for which the ungated system supports anti-phase (respectively, in-phase) oscillations. The colored solid curves enclose the set of $(D, \overline{\kappa})$ values for which the gated system supports anti-phase oscillations for various choices of the switching rates. As described in the text, if $\alpha/\beta \gg 1$ (orange curve) or $\alpha + \beta \gg 1$ (blue curve), the anti-phase region of the gated system approaches the anti-phase region of the ungated systen. Further, if $\alpha/\beta \ll 1$ (green curve), then the anti-phase region of the gated system approaches the in-phase region of the gated system. For intermediate values of α and β (red curve), the anti-phase region of the gated system seems to interpolate the anti-phase and in-phase regions of the ungated system. Importantly, for intermediate values of α and β, there exists parameter choices (red circle) where the gated system supports oscillations, but the ungated system does not, and there exists parameter choices (black circle) where the ungated system supports oscillations, but the gated system does not. These are confirmed by simulations of the full system in Figs. 5 and 6. As described in the text, the set of $(D, \overline{\kappa})$ values for which the gated system supports in-phase oscillations is the same as for the ungated system.

the ungated system does not. Conversely, there exists parameter regimes where the ungated system exhibits oscillations, but the gated system does not. For example, Fig. 4 shows that if $\alpha = 1$, $\beta = 10$, $D = 0.65$, and $\overline{\kappa} = 0.5$, then the gated system supports only anti-phase oscillations, but the ungated system does not support any oscillations. On the other hand, if $\alpha = 1$, $\beta = 10$, $D = 0.4$, and $\overline{\kappa} = 0.485$, then the ungated system supports only anti-phase oscillations, but the gated system does not support any oscillations.

The predictions of our analysis agree with stochastic simulations of the full nonlinear coupled PDE-ODE system in (2.1). In Fig. 5, we plot a simulation of a single realization of the stochastically gated system with $\alpha = 1$, $\beta = 10$, $D = 0.65$, and $\overline{\kappa} = 0.5$, along with a simulation of the ungated system for the same parameters. We see that the stochastic system exhibits anti-phase stochastic

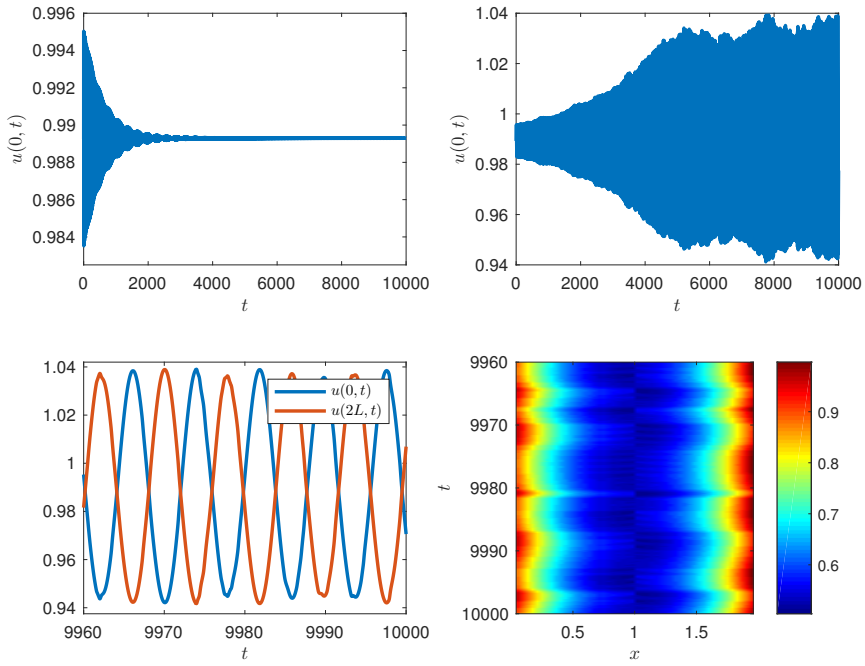

Figure 5: Simulations of the full nonlinear coupled PDE-ODE system: There exists parameter choices where the ungated system does not support oscillations, but the stochastically gated system does. Here, $D = 0.65$ and $\overline{\kappa} = 0.5$, and other parameters are as in the caption of Fig. 3. Given a small perturbation about the steady state at $t = 0$, the upper left panel shows that the ungated system decays to a steady state, but the right panel shows that the stochastically gated system oscillates. Zooming in on this realization of the stochastic system, the bottom left panel reveals that these stochastic oscillations are indeed anti-phase. The bottom right panel plots $u(x,t)$ for the gated system over a set of large times.

oscillations, but the ungated system decays to a steady state. Conversely, in Fig. 6, we plot a simulation of a single realization of the stochastically gated system with $\alpha = 1$, $\beta = 10$, $D = 0.4$, and $\overline{\kappa} = 0.485$, along with a simulation of the ungated system for the same parameters. There, we see that the stochastic system decays to a steady state, but the ungated system exhibits anti-phase oscillations.

Finally, we describe our numerical implementation of the full nonlinear coupled PDE-ODE stochastic system. For a given stochastic simulation, we first generated the sequence of holding times of the Markov process, $n(t)$. That is, to simulate the system until some given terminal time T_{end} (in the case of Figs. 5 and 6, the terminal time was $T_{\text{end}} = 1000$), we first generated a sequence of independent and identically distributed exponential random variables, $\{\tau_0, \tau_1^k\}_{k=1}^K$, with τ_0^k and τ_1^k having rate parameters β and α, and the random variable K is

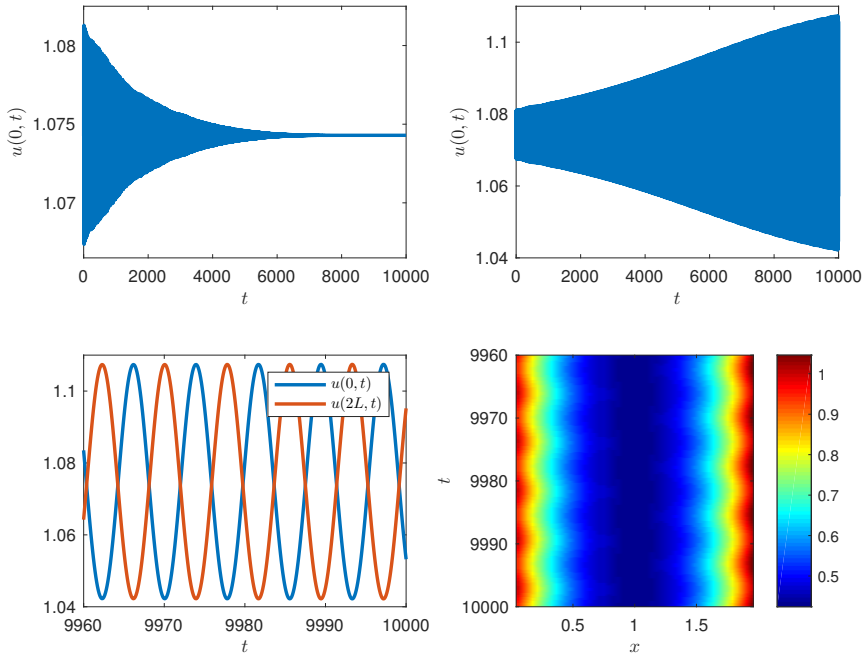

Figure 6: Simulations of the full nonlinear coupled PDE-ODE system: There exists parameter choices where the stochastically gated system does not support oscillations, but the ungated system does. Here, $D = 0.4$ and $\overline{\kappa} = 0.485$, and other parameters are as in the caption of Fig. 3. Given a small perturbation about the steady state at $t = 0$, the upper left panel shows that the stochastically gated system decays to a steady state, but the right panel shows that the ungated system oscillates. Zooming in on this realization of the ungated system, the bottom left panel reveals that these oscillations are indeed anti-phase. The bottom right panel plots $u(x,t)$ for the ungated system over a set of large times.

$K = \inf\{k' : \sum_{k=1}^{k'}(\tau_0^k + \tau_1^k) > T_{\text{end}}\}$. Hence, the statistics of the jump times of $n(t)$ are exact. To simulate the evolution of the system between jumps of $n(t)$, we discretized the spatial domain $[0, 2L]$ and used the method of lines. The details of this method are given above in our derivation of the first moment equations (3.16a)-(3.16b), though we applied this method to the full nonlinear system (not the linearized version considered above). We used 100 spatial grid points (a finer spatial discretization yielded the same qualitative results). To solve the resulting system of ODEs (an ODE for each spatial grid point and ODEs for V_r, W_r), we used stiff ODE solvers that were built-in to MATLAB [31], having set the maximum allowable time step to be 0.1 (smaller maximum time steps yielded the same qualitative results).

4. Discussion

In this paper, we combined work on diffusion in domains with randomly switching boundaries [27, 3, 7, 8] and studies of diffusively-coupled active biochemical oscillators [21, 22]. This was motivated by the particular problem of a pair of cells with active membranes coupled via a stochastically-gated gap junction. The resulting system is described by a stochastic (piecewise-deterministic) PDE-ODE. Linearizing about a deterministic steady-state solution, we investigated the existence of in-phase and anti-phase oscillations by solving the spectral problem for a linear operator obtained by averaging over realizations of the stochastic gate. We thus showed how the gate has a non-trivial effect on the existence of the anti-phase solution.

It is important to point out that the amplitudes of the oscillations in Figs. 5 and 6 are small. However, in this paper we are mainly interested in establishing the principle of noise-induced or noise-suppressed oscillations. In order to determine whether or not such phenomena could be observed in the real noisy environment of cells, one would require a more extensive parameter search using a variety of different ODE models. In particular, it is known that certain biochemical networks exhibit ultrasensitivity to inputs [9], whereby small changes in input lead to large changes in response. It would be interesting to determine whether or not such an amplification mechanism could enhance the effects identified in our paper.

As far as we are aware, there are currently no experimental studies exploring the combined effects of bulk diffusion and stochastic gap junctions on coupled biochemical oscillators. In particular, it is not known whether the resulting oscillations are in-phase or anti-phase. However, there is an interesting example of anti-phase oscillations, which occurs during cell polarization in fission yeast. Fission yeast is a rod-shaped cell consisting of two hemispheres of constant radius that cap a cylinder of increasing length. There are two distinct stages of axial cell growth: immediately following cell division, the cell initially grows at one end only, namely, the "old end" of the previous cell cycle (monopolar growth). However, at a critical length, the cell also starts growing from the new end (bipolar growth), in a process known as "new end take off" (NETO) [14]. It has been found experimentally that the signaling molecule Rho GTPase Cdc42, which plays an important role in regulating cell polarization, exhibits oscillations with an average period of 5 min [13]. Moreover, oscillations occur at both ends of the cell and are anti–phase. In the case of longer cells exhibiting bipolar growth, the mean amplitude of the oscillations were the same at both ends (symmetric, anti-phase oscillations). On the other hand, for shorter, less mature cells exhibiting monopolar growth, the amplitude was significantly larger at the growing end (asymmetric, anti-phase oscillations). These experimental observations have recently been reproduced in a mathematical model in the form of a PDE-DDE system on a growing domain [39].

More broadly, our work contributes to the analysis of piecewise deterministic Markov processes (PDMPs), which are also known as dichotomous noise processes in the physics literature [1]. Such processes are finding an increasing num-

ber of applications in biology, including to gene networks, neuroscience, chemotaxis, ion channels, and motor-driven intracellular transport [2, 10, 15, 16, 35]. A distinguishing feature of the present work is that our system evolves according to a PDE in between jumps of the Markov process, whereas the vast majority of previous work on PDMPs has tended to consider only ODE evolution between Markov jumps.

There are a number of possible extensions of our work. First, we could derive linear PDE-ODEs for second-order (and higher-order) moments of the stochastic perturbations. These would be obtained by multiplying the CK equation (3.8) by products of the concentrations, performing integration by parts, and then retaking the continuum limit. In the case of second-order moments we would obtain dynamical equations for the two-point, equal-time correlations

$$\Lambda_n^{cc}(x,y,t) = \mathbb{E}[c(x,t)c(y,t)1_{n(t)=n}],\ \Lambda_{n,r}^{c\varphi}(x,t) = \mathbb{E}[\varphi_r(t)c(x,t)1_{n(t)=n}],$$
$$\Lambda_{n,r}^{c\phi}(x,t) = \mathbb{E}[\phi_r(t)c(x,t)1_{n(t)=n}],\quad \Lambda_{n,rs}^{\varphi\varphi}(x,t) = \mathbb{E}[\varphi_r(t)\varphi_s(t)1_{n(t)=n}],$$
$$\Lambda_{n,rs}^{\phi\phi}(t) = \mathbb{E}[\phi_r(t)\phi_s(t)1_{n(t)=n}],\quad \Lambda_{n,rs}^{\varphi\phi}(t) = \mathbb{E}[\varphi_r(t)\phi_s(t)1_{n(t)=n}]$$

Note, in particular, that $\Lambda_n^{cc}(x,y,t)$ would satisfy a two-dimensional parabolic PDE. However, the resulting spectral problem rapidly becomes analytically intractable so one would need to develop efficient numerical schemes. At least for the parameter values considered in this paper, higher-order moments do not appear to blow-up, suggesting that the first-moment spectral problem is a good predictor of the existence of diffusion-induced oscillations. We hope to develop a more rigorous analysis of stability in future work.

More theoretical extensions would be to investigate some of the subtle mathematical questions raised by this study. First, while our restricted stability criterion was confirmed by numerics, there is the question of its rigorous justification. Second, it would be useful to develop our stochastic averaging approach for nonlinear PDE. In particular, we had to first linearize the system in order to find first moment equations. Third, there is the question of a detailed investigation into the types of PDEs that are amenable to the spatial discretization approach that we used in section 3 to derive the first moment system. Fourth, one would like to extend our methods to allow the opening and closing rates, α and β, to depend on the concentrations of diffusing molecules. Of course, this is more than a mathematical curiosity, since channel gating is voltage dependent [11].

One final extension would be to take into account the fact that gap junctions tend to have a finite permeability [25]. This would mean that at the intercellular boundary $x = L$, the concentration of the signaling molecule is discontinuous. Conservation of diffusive flux across the boundary would imply that the boundary condition (2.1c) for $n(t) = 0$ would become

$$-D\frac{\partial u(L^-,t)}{\partial x} = -D\frac{\partial u(L^+,t)}{\partial x} = \mu[u(L^-,t) - u(L^+,t)].$$

However, it could be argued that at least a partial contribution to the effective permeability arises from the random opening and closing of the gap junction.

Yet another extension would be to consider more general geometric configurations of cells. For example, Keener and Sneyd [25] have previously considered a line of two-dimensional cells with gap-junctional openings in the connecting edges. Using symmetry arguments, they showed how the gap junctions along an edge can be lumped into a single effective junction at the center of each edge. Incorporating such a configuration into our framework would require understanding how the membrane of a two-dimensional (or three-dimensional) cell is partitioned into active membrane domains and gap junctions.

References

[1] I. Bena. Dichotomous Markov noise: exact results for out-of-equilibrium systems. Int. J. Mod. Phys. B 20 2825-2888 (2006).

[2] P. C. Bressloff. Stochastic processes in cell biology. Springer, New York (2014).

[3] P. C. Bressloff and S. D. Lawley. Moment equations for a piecewise deterministic PDE. J. Phys. A 48 (2015) 105001.

[4] P. C. Bressloff and S. D. Lawley. Stochastically-gated diffusion-limited reactions for a small target in a bounded domain. Phys. Rev. E. 92 (2015).

[5] P. C. Bressloff and S. D. Lawley. Escape from a potential well with a switching boundary. J. Phys. A 48 (2015) 225001.

[6] P. C. Bressloff and S. D. Lawley. Escape from subcellular domains with randomly switching boundaries. Multiscale Model. Simul., 13 (2015) 1420-1455.

[7] P. C. Bressloff. Diffusion in Cells with stochastically-gated gap junctions. SIAM J. Appl. Math 76 (2016) 1658-1682.

[8] P. C. Bressloff and S. D. Lawley. Diffusion on a tree with stochastically gated nodes. J. Phys. A 49 (2016) 245601.

[9] P. C. Bressloff. Ultrasensitivity and noise amplification in a model of v. harveyi quorum sensing, Phys. Rev. E 93 (2016) 062418.

[10] P. C. Bressloff. Stochastic Liouville equation for particles driven by dichotomous environmental noise. Phys. Rev. E 95 (2017) 012124.

[11] F. K. Bukauskas and V. K. Verselis. Gap junction channel gating. Biochim. Biophys. Acta 1662 (2004) 42-60.

[12] B. W. Connors and M. A. Long. Electrical synapses in the mammalian brain. Ann. Rev. Neurosci. 27 (2004) 393-418.

[13] M. Das, T. Drake, D. J. Wiley, P. Buchwald, D. Vavylonis, and F. Verde, Oscillatory dynamics of Cdc42 GTPase in the control of polarized growth. Science 337 (2012) 239–243.

[14] T. Drake and D. Vavylonis Cytoskeletal dynamics in fission yeast: a review of models for polarization and division. HFSP J. 4 (2010) 122-130.

[15] F. Droste and B. Lindner. Integrate-and-fire neurons driven by asymmetric dichotomous noise. Biol. Cybern. 108.6 (2014) 825–843.

[16] B. Ermentrout. Computational Modeling of Genetic and Biochemical Networks: Simplifying and reducing complex models. MIT Press (2011) 307–323.

[17] W. J. Evans and P. E. Martin. Gap junctions: structure and function. Mol. Membr. Biol. 19 (2002) 121-136.

[18] C. W. Gardiner. Handbook of stochastic methods, 4th edition. Springer, Berlin (2009).

[19] A. Gomez-Marin, J. Garcia-Ojalvo, J. M. Sancho. Self-sustained spatiotemporal oscillations induced by membrane-bulk coupling, Phys. Rev. Lett. 98 (16) (2007) 168303.

[20] D. A. Goodenough and D. L. Paul. Gap junctions. Cold Spring Harb Perspect Biol 1 (2009) a002576

[21] J. Gou, Y-X Li, W. Nagata and M. J. Ward. Synchronized oscillatory dynamics for a 1-D model of membrane kinetics coupled by linear bulk diffusion. SIAM J. Appl. Dyn. Sys., 14 (2015) 2096–2137.

[22] J. Gou and M. J. Ward. Oscillatory dynamics for a coupled membrane-bulk diffusion model with Fitzhugh-Nagumo kinetics. SIAM J. Appl. Math. 76 (2) (2016) 776–804.

[23] J. Gou, M. Ward. An asymptotic analysis of a 2-d model of dynamically active compartments coupled by bulk diffusion. J. Nonlin. Sci. 26 (2016) 979-1029.

[24] J. Gou, W.-Y. Chiang, P.-Y. Lai, M. J. Ward and Y.-X. Li. A theory of synchrony by coupling through a diffusive chemical signal. Physica D. 339 (2017) 1-17.

[25] J. P. Keener and J. Sneyd. Mathematical Physiology I: Cellular Physiology, 2nd edn. Springer, New York (2009)

[26] I. Klapper and J. Dockery Mathematical description of microbial biofilms. SIAM Rev. 52 (2010) 221–265.

[27] S. D. Lawley, J. C. Mattingly and M. C. Reed. Stochastic switching in infinite dimensions with applications to random parabolic PDE. SIAM J. Math. Anal. 47 (2015) 3035-3063

[28] S. D. Lawley and J. P. Keener. A new derivation of Robin boundary conditions through homogenization of a stochastically switching boundary. SIAM J. Appl. Dyn. Syst. 14 (2015) 1845-1867

[29] S. D. Lawley. Boundary value problems for statistics of diffusion in a randomly switching environment: PDE and SDE perspectives. SIAM J. Appl. Dyn. Syst. 15 (2016) 1410-1433.

[30] S. D. Lawley, J. A. Best and M. C. Reed. Neurotransmitter concentrations in the presence of neural switching in one dimension. Disc. Contin. Dyn. Syst. Ser. B, 21 (2016) 2255-2273.

[31] MATLAB Release 2015b, The MathWorks, Inc., Natick, Massachusetts, United States.

[32] M. B. Miller, B. L. Bassler. Quorum sensing in bacteria. Ann. Rev. Microbiol. 55 (1) (2001) 165–199.

[33] J. Müller, C. Kuttler, B. A. Hense, M. Rothballer, A. Hartmann. Cell–cell communication by quorum sensing and dimension-reduction. J. Math. Biol. 53 (4) (2006) 672–702.

[34] J. Müller, H. Uecker. Approximating the dynamics of communicating cells in a diffusive medium by ODES—homogenization with localization. J. Math. Biol. 67 (5) (2013) 1023–1065.

[35] H. G. Othmer and T. Hillen. The diffusion limit of transport equations derived from velocity-jump processes. SIAM J. Appl. Math. 61 (3) (2000): 751–775.

[36] J. C. Saez, V. M. Berthoud, M. C. Branes, A. D. Martinez and E. C. Beyer. Plasma membrane channels formed by connexins: their regulation and functions. Physiol. Rev. 83 (2003) 1359–1400 (2003)

[37] S. Y. Shvartsman, E. Shütz, R. Imbihl, I. G. Kevrekidis. Dynamics on microcomposite catalytic surfaces: the effect of active boundaries, Phys. Rev. Lett. 83 (1999) 2857-2861.

[38] C. M. Waters and B. L. Basser Quorum sensing: Cell-to-cell communication in bacteria. Annu. Rev. Cell Dev. Biol. 21 (2005) 319-346.

[39] B. Xu and P. C. Bressloff. A PDE-DDE model for cell polarization in fission yeast. SIAM J. Appl. Math 76 (2016) 1844-1870.

[40] B. Xu and P. C. Bressloff. A theory of synchrony for active compartments with delays coupled through bulk diffusion. Physica D 341 (2017) 45-59.